

# Investigation of Competitive Adsorption Properties of CO/CO<sub>2</sub>/O<sub>2</sub> onto the Kailuan Coals by Molecular Simulation

Xuanmeng Dong, Fusheng Wang, Liwen Guo, Yu Zhang, and Xianwei Dong\*



Cite This: *ACS Omega* 2022, 7, 19305–19318



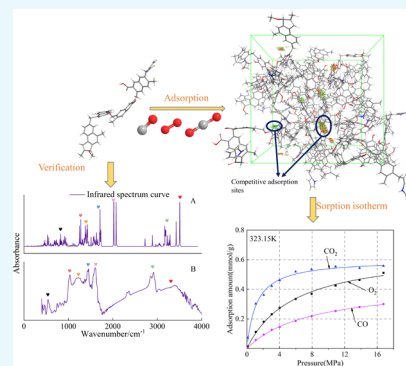
Read Online

ACCESS |

Metrics & More

Article Recommendations

**ABSTRACT:** To reveal the CO, CO<sub>2</sub>, and O<sub>2</sub> adsorption properties of two bituminous coals at different pressures and temperatures, the molecular unit-cell structures of two types of bituminous coal are constructed (C<sub>1180</sub>H<sub>960</sub>O<sub>120</sub>N<sub>20</sub> and C<sub>1160</sub>H<sub>860</sub>O<sub>80</sub>N<sub>20</sub>) by Fourier transform infrared (FTIR) spectroscopy. The bituminous coal molecular FTIR spectroscopic curve is calculated by quantum chemistry, and the results are consistent with the experimental curve. The isothermal adsorption curves of the single-component gases CO, CO<sub>2</sub>, and O<sub>2</sub> conform to the Langmuir equation from 20 to 60 °C. The adsorption simulations are mainly performed using grand canonical Monte Carlo (GCMC) methods. The amount of adsorption decreases with increasing temperature at the same pressure, and CO<sub>2</sub> can be the first to reach adsorption saturation at the same temperature. The CO<sub>2</sub>/CO adsorption selectivity for binary gas mixtures has apparent advantages in low-pressure or shallow buried coal seams. The adsorption selectivity of O<sub>2</sub>/CO varying under different pressures is not obvious. The high amount of CO inhibits the adsorption capacity of CO<sub>2</sub> and O<sub>2</sub>. In other words, the effect of injecting CO<sub>2</sub> to control fire extinguishing in bituminous coal seams with high abnormal CO concentrations is not significant.



## 1. INTRODUCTION

Bituminous coal is the most widely distributed coal in nature.<sup>1</sup> It is mainly distributed in northern provinces (autonomous regions) in China, of which the bituminous coal reserves in North China account for more than 60% of the national reserves. Coal seams are prone to oxidative spontaneous combustion during mining and operations, which increases the risk of fire accidents. It is necessary to study the microstructure of coal to explore its adsorption mechanism and ignition mechanism.<sup>2–4</sup> The differences in the coal structure affect the permeation and adsorption of coalbed methane (CBM) in coal seams.<sup>5</sup> Chen et al.,<sup>6</sup> Chen et al.,<sup>7</sup> and Solomon et al.<sup>8</sup> used the analytical technique of Fourier transform infrared (FTIR) spectroscopy to determine the molecular differences in coal. The ability of coal with different molecular structures to adsorb gases differs.<sup>9,10</sup> O<sub>2</sub> is the dominant factor in the violent reaction stage of spontaneous coal combustion.<sup>11–13</sup> However, O<sub>2</sub> is physically adsorbed on the surface of coal functional groups before participating in the coal oxygen reaction. To prevent O<sub>2</sub> from reaching saturation adsorption and participating in chemical reactions, Fang et al.<sup>14</sup> designed an experiment to displace O<sub>2</sub> with inert gas. Li<sup>15</sup> and Chen et al.<sup>16</sup> used experiments to determine the physical adsorption of O<sub>2</sub> by lignite. They concluded that the oxygen uptake of coals with a low metamorphic and large specific surface area has higher oxygen absorption. Lu et al.<sup>17</sup> and Cheng et al.<sup>18</sup> found that O<sub>2</sub> was mainly adsorbed by van der Waals forces and compared the adsorption states of CO<sub>2</sub>, O<sub>2</sub>, and other small molecules in

lignite. CO<sub>2</sub> is the greenhouse gas generated by the coal oxidation reaction and a common fire extinguishing component.<sup>19</sup> Wu et al.<sup>20</sup> used the grand canonical Monte Carlo (GCMC) method to simulate and compare CO<sub>2</sub> and O<sub>2</sub>. CO<sub>2</sub> is adsorbed by van der Waals forces and electrostatic action, so the competitiveness is usually CO<sub>2</sub> > O<sub>2</sub>. Most scholars generally compare the competition and adsorption laws between CO<sub>2</sub> and CH<sub>4</sub>. Zhou et al.,<sup>21,22</sup> Gao et al.,<sup>23</sup> Wang et al.,<sup>24</sup> Zhang et al.,<sup>25</sup> Ding,<sup>26</sup> and Sui et al.<sup>27,28</sup> discussed the competitive adsorption behavior of CO<sub>2</sub> and CH<sub>4</sub> in lignite or organic matter. However, for some mines with abnormal CO sources, the change in the CO index gas should be given more attention. Therefore, Zhu et al.<sup>29</sup> and Zhang et al.<sup>30</sup> used experimental instruments to analyze the performance of coal adsorbing CO. Deng et al.<sup>31,32</sup> simulated the explosion process and the explosion concentration limit of CH<sub>4</sub> and CO mixtures based on experiments. Zhou<sup>33</sup> used quantum chemistry to calculate the adsorption characteristics of CO and CO<sub>2</sub> on the coal surface, clarified the competitive adsorption process of CO mixed with other gases, and found that the affinity sequence of adsorption is CO<sub>2</sub> > CO.

Received: February 11, 2022

Accepted: May 20, 2022

Published: June 1, 2022



**Table 1. Proximate and Ultimate Analysis of Bituminous Coal Samples<sup>a</sup>**

coal samples	proximate analysis				total sulfur	ultimate analysis			
	M <sub>ad</sub> (%)	A <sub>d</sub> (%)	V <sub>daf</sub> (%)	FC <sub>d</sub> (%)		O <sub>daf</sub> (%)	C <sub>daf</sub> (%)	H <sub>daf</sub> (%)	N <sub>daf</sub> (%)
no. 1 coal	1.93	8.27	41.43	53.73	0.51	11.79	80.90	5.28	1.47
no. 2 coal	0.65	15.75	28.39	60.33	0.52	7.59	85.24	4.83	1.72

<sup>a</sup>Nomenclature: M<sub>ad</sub> represents moisture on an air dry basis; A<sub>d</sub> represents ash on a dry basis; V<sub>daf</sub> represents volatile on a dry ash free basis; FC<sub>d</sub> represents fixed carbon; S<sub>td</sub> stands for total sulfur on a dry basis; and O<sub>daf</sub>, C<sub>daf</sub>, H<sub>daf</sub>, and N<sub>daf</sub> represent the percentages of oxygen, carbon, hydrogen, and nitrogen elements, respectively.

The source of underground CO is oxidation, spontaneous combustion, and the original CO in coal,<sup>34–36</sup> which scholars have verified. The original CO in coal formation will also make CO exceed the standard of security. However, coal mine safety regulations stipulate that the maximum allowable value of the underground CO concentration is 0.0024%.<sup>37</sup> It is also common to use CO as an index gas to determine coal seam spontaneous combustion in the actual production process.<sup>38,39</sup> Therefore, it is necessary to study the adsorption of CO in coal. Although Zhang et al.<sup>40</sup> analyzed the competition between CO and other small molecules in lignite by molecular simulation, there is a lack of comparison of adsorption selectivity between CO and other small molecules.

Therefore, we aimed to clarify the competitive characteristics and adsorption capacity between O<sub>2</sub>, CO<sub>2</sub>, and CO of bituminous coal, aiming at the occurrence and diffusion behavior of CO in coal seams. The molecular structure parameters were calculated by Fourier infrared spectroscopy experiments, and a simplified molecular model and supercell structure of two types of bituminous coal were constructed. The adsorption capacity of the single-component gases CO, CO<sub>2</sub>, and O<sub>2</sub> in the adsorption system under different temperatures and burial depths was compared. The difference in gas adsorbed by different bituminous coals was analyzed. The binary adsorption competition relationship between CO, CO<sub>2</sub>, and O<sub>2</sub> was simulated to obtain the adsorption selectivity of CO, CO<sub>2</sub>, and O<sub>2</sub> at different concentrations and compare the adsorption selectivity at different pressures. This study provides a theoretical basis for mine CO anomalies and coal spontaneous combustion fire prevention.

## 2. TEST AND SIMULATION

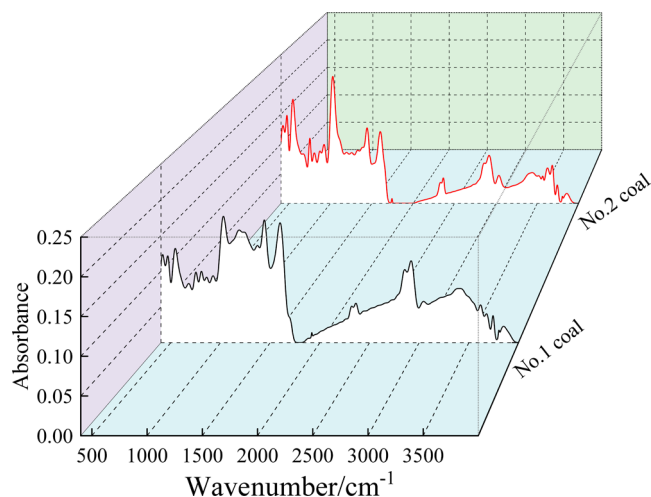
**2.1. Experiment.** **2.1.1. Proximate and Elemental Analysis.** Fresh coal samples of mine working faces are collected according to the standard coal seam sampling method (GB/T 482-2008), and two coal types with different coal ranks are selected for experimental analysis. No. 1 and 2 coals are mined from the Linnancang and Qianjiaying mining areas.<sup>41</sup> The coal sample particle size was controlled below 200 mesh by crushing, screening, and grinding. Samples were placed into sealed bags and labeled. A Vario El III organic element tester and an automatic sulfur tester were used to measure the proportion of major elements in the coal samples.<sup>42</sup> A large gap resulted when the SE-MAG6700 automatic industrial analyzer was used in the industrial analysis because of the influence of experimental conditions. Therefore, based on the industrial analysis method of coal (GB/T 212-2008), naturally dried coal with no additional moisture removal was taken as the reference coal, and the particle size was controlled to below 0.2 mm.

According to the national standard for coal classification in China (GB5751-86), no. 1 and 2 coal samples are gas coal and coking coal, both of which are bituminous coals. The moisture, ash, and various element compositions of the two coal samples

are shown in Table 1. Under high-temperature conditions, small molecular side chains and active oxygen-containing functional groups in the coal molecular structure produce substances, such as H<sub>2</sub>O and CO<sub>2</sub>. Therefore, when the degree of coalification increases, polycondensation of the molecular structure of coal reduces the number of decomposition products that are formed during the thermal reaction. The volatile content of no. 1 coal is 41.43% and that of no. 2 coal is 28.39%. No. 1 coal has a low coalification degree and a high volatile content, and the percentage of fixed carbon and elemental carbon is less than that of no. 2 coal. Because of the high rank, the coal density increases, the pores are poorly developed, the specific surface area decreases, the carbon condensation level increases, the number of functional groups of high metamorphic coal relative to the low metamorphic coal decreases, and the water-absorption capacity is inferior to that of the low metamorphic coal.

**2.1.2. Fourier Transform Infrared Spectroscopy Experiment.** Coal samples with a particle diameter below 200 mesh were mixed completely with KBr. The halogenating agent tablet pressing method was selected for the infrared spectrum test on a Shimadzu FTIR-8400 FTIR spectrometer made in Japan. The main parameters were set as follows: the image resolution was 4.0 cm<sup>-1</sup>, the wavenumber was varied between 400 and 4000 cm<sup>-1</sup>, each coal sample was scanned 30 times, the two coals were analyzed by FTIR, and the absorbance curve that corresponds to each wavenumber was obtained.<sup>43</sup>

The functional group region in the infrared spectrum is 1300–4000 cm<sup>-1</sup>, and the wavenumber in the fingerprint region is 650–1300 cm<sup>-1</sup>. The infrared fingerprint region is like a human fingerprint and represents the characteristic peaks of some functional groups to distinguish subtle differences in the material structure. Figure 1 shows the trend chart of the peak

**Figure 1.** FTIR spectrum of experimental coal samples.

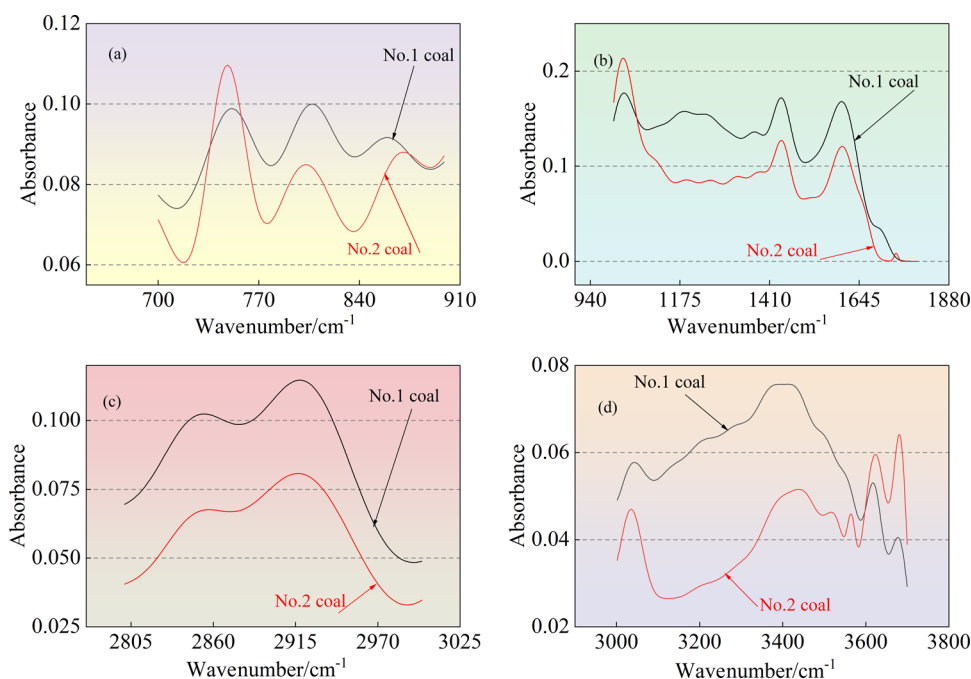


**Figure 2.** FTIR segmented spectra of coal samples. (a) Aromatic-ring-substituted hydrogen in the range of 700–900  $\text{cm}^{-1}$ , (b) characteristic functional groups of 1000–1800  $\text{cm}^{-1}$ , (c) aliphatic hydrocarbon absorption zone of 2800–3000  $\text{cm}^{-1}$ , and (d) hydroxyl or hydrogen bond absorption peak groups of 3000–3700  $\text{cm}^{-1}$ .

spectra of the coal samples after baseline calibration. The metamorphic degree of the coal sample affects the shape and position of the absorption peak. In the fingerprint area, the absorption peak is 700–900  $\text{cm}^{-1}$ , which represents the change in the aromatic ring. The absorbance tends to increase with an increase in the coalification degree. The region 1000–1300  $\text{cm}^{-1}$  represents ether bond destruction and recombination. In the functional group area, the peak pattern that corresponds to the same wavenumber in the curve in Figure 1 shows that the aliphatic side chain, the oxygen-containing functional group, and the hydrogen bond changed, and differences existed in the structure of the two bituminous coals.

The segmented FTIR spectra of the coal are compared and calculated quantitatively by peak fitting so that the peak group with a wavenumber of 400–4000  $\text{cm}^{-1}$  is divided into four regions. Figure 2a shows aromatic-ring-substituted hydrogen in the range of 700–900  $\text{cm}^{-1}$ . The characteristic functional groups of 1000–1800  $\text{cm}^{-1}$  are shown in Figure 2b. Figure 2c shows the aliphatic hydrocarbon absorption zone of 2800–3000  $\text{cm}^{-1}$ . Figure 2d shows hydroxyl or hydrogen bond absorption peak groups of 3000–3700  $\text{cm}^{-1}$ .<sup>44</sup>

As shown in Figure 2a, the peak number of two bituminous coals at 700–900  $\text{cm}^{-1}$  is 3, and the absorbance of no. 2 coal increased significantly at  $\sim 750$   $\text{cm}^{-1}$ . In Figure 2b, the absorbance of no. 2 coal at  $\sim 1025$   $\text{cm}^{-1}$  is greater than that of no. 1 coal. Continuous peaks occurred at  $\sim 1185$  and  $1250$   $\text{cm}^{-1}$ , and the peak intensity was weak. Shoulder peaks occurred at  $\sim 1370$   $\text{cm}^{-1}$ , and two peaks existed near  $1440$  and  $1600$   $\text{cm}^{-1}$ . After a weak peak appears near  $1740$   $\text{cm}^{-1}$ , the absorbance of the two coals gradually approached 0. In Figure 2c, the absorbance curves of the two coal samples are roughly parallel without intersection. At the same wavenumber, the absorbance of the higher metamorphic coal is less than that of the lower metamorphic coal. Two broad peaks formed at  $\sim 2851$  and  $2918$   $\text{cm}^{-1}$ . At  $2851$   $\text{cm}^{-1}$ , the peak of no. 2 coal is lower than that of no. 1 coal, which indicates that fewer methylene groups

are present. At  $2918$ – $3000$   $\text{cm}^{-1}$ , the slope of the absorbance curve of no. 2 coal is less than that of no. 1 coal, which indicates that a large methyl content exists in no. 2 coal. In Figure 2d, at  $\sim 3034$   $\text{cm}^{-1}$ , the peak shape of no. 2 coal is sharper than that of no. 1 coal. At  $\sim 3435$   $\text{cm}^{-1}$ , the peak neck of no. 1 coal is longer than that of no. 2 coal and the peak shoulder is wider than that of no. 2 coal. Accounting for the high metamorphic degree of no. 2 coal, the number of fused rings increases because of carbon condensation during coalification, which reduces the spatial distance of the hydroxyl groups and continuously formed self-associated hydrogen bonds. The weak peak at  $\sim 3518$   $\text{cm}^{-1}$  belongs to the hydrogen bond that is composed of a hydroxyl and a  $\pi$  bond.

In Figures 3–5, (a) represents no. 1 coal and (b) represents no. 2 coal. The baseline of the peak fitting is consistent, the fitting degree  $R^2 > 99.6\%$ , and all peaks are Gaussian.

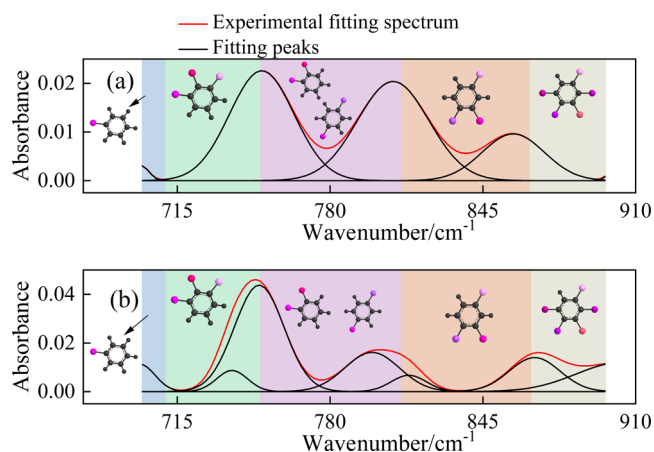


**Figure 3.** FTIR spectra of aromatic substituted hydrogen in coal. (a) no. 1 coal and (b) no. 2 coal.

**Table 2. Attribution of Absorption Peaks in FTIR Spectra**

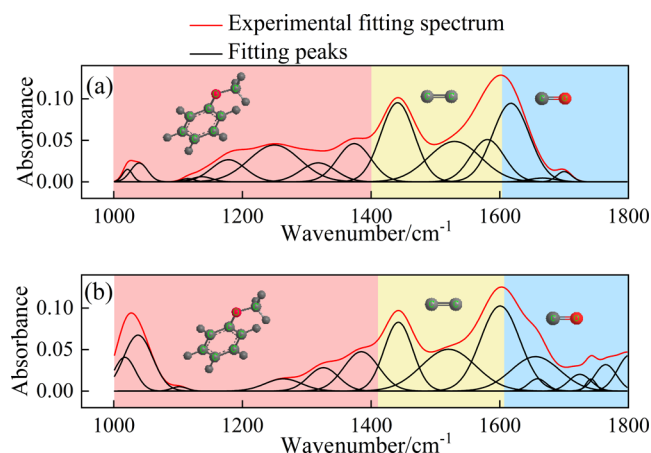
wavenumber/cm <sup>-1</sup>	690–710	710–750	750–810	810–865	865–900
absorption peak type	mono-substitution	1,2,3 tri-substitution	di-substitution	1,3,5 tri-substitution	penta-substitution

Four aromatic ring-substitution types existed in the experimental coal samples, namely mono-, di-, tri-, and penta-substitution, and the corresponding wavenumbers are shown in Table 2. The change in the coal aromatic structure is shown in Figure 3. The single substitution contents of no. 1 and 2 coal are 1.3 and 5.8%, respectively. The main mode of no. 1 coal is meta-di-substitution, with a content of 81.6%. No. 2 coal is mainly mono-, di-, and trisubstituted, with a content of 43.1%. No peak sample existed in the wavenumber range of 710–750 cm<sup>-1</sup> for no. 1 coal. The algebraic quantity of mono-, tri-, and pentasubstituted no. 1 coal is 12.6% more than that of no. 2 coal, and the pentasubstituted content of no. 2 coal is 31.1% more than that of no. 1 coal. Therefore, a high rank of bituminous coal yields more substitution sites with a more stable structure and a greater ring-forming rate. The substitution site content changes from double to tri- and penta-substitution because of the disconnection of C–H bonds of the aromatic ring and substitution by some atoms or groups, dehydrogenation of naphthenic aliphatic hydrocarbons into rings, dehydrogenation of aromatic ring branches, and dehydroxylation and decarboxylation of the benzene structure.<sup>45</sup>

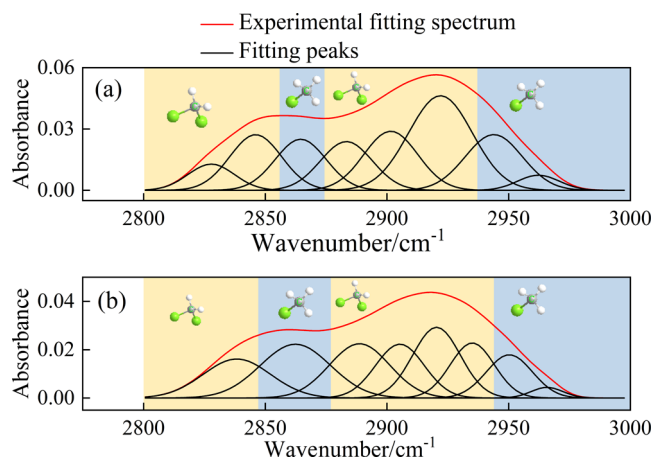
The characteristic atoms or atomic groups in coal include ether bonds, carbonyls, carboxyls, hydroxyls, esters, and anhydrides. The wavenumber range of the main characteristic functional groups is 1000–1800 cm<sup>-1</sup>,<sup>46</sup> including symmetric and antisymmetric stretching vibrations, such as C–O, C=O, and C=C bonds.<sup>47</sup> Figure 4 shows the number of oxygen-

4.5 and 7.1%, respectively. The peak area of no. 1 coal is 8.9% at 1330–1390 cm<sup>-1</sup>. The peak position of ~1666 cm<sup>-1</sup> belongs to the diaryl ketone structure and the peak position of 1700 cm<sup>-1</sup> belongs to the aromatic ketone structure. The two peaks are close to each other and belong to the C=O bond vibration peak of ketones. The C=O bond of the 1650–1660 and 1700–1740 cm<sup>-1</sup> band in the –COOH group in no. 2 coal is telescopic vibration, and the relative areas of the two bands are 11.6 and 2.3%. C=O of no. 2 coal has peaks near 1740–1750 and 1750–1800 cm<sup>-1</sup>. The former belongs to five-membered cyclic ketones and the latter belongs to five-membered cyclic anhydrides, in which the C=O bond vibrates symmetrically. The 1441, 1529, 1580, and 1617 cm<sup>-1</sup> peaks in no. 1 coal and 1442, 1520, and 1600 cm<sup>-1</sup> peaks in no. 2 coal belong to the internal skeleton vibration of C=C, and the peak areas are 62.7 and 46.3%. The 1373 and 1384 cm<sup>-1</sup> peak positions of no. 1 and 2 coal belong to the in-plane bending vibration of phenolic –OH, and there is a little difference in the peak area between them. The calculated saturated C–O vibration peak area of no. 1 coal is 31.0%, including phenol carbon (C–OH) at 8.9% and ether carbon (C–O–C) at 22.2%. The peak area of unsaturated C=O is 6.3%, including ketones and carboxylic acids. The ratio of saturated C–O to unsaturated C=O is ~5:1, and the ratio of phenol carbon to ether carbon is ~2:5. The ratio of saturated C–O to unsaturated C=O of no. 2 coal is ~1:1.28, in which the ratio of the five-membered cyclic anhydride structure to the number of C=O bonds is ~1:2.65.

The peak spectra of small molecular aliphatic hydrocarbon groups of bituminous coals with two metamorphic degrees are shown in Figure 5, which are divided into eight peaks in the

**Figure 4.** FTIR spectra of characteristic functional groups of coal. (a) no. 1 coal and (b) no. 2 coal.

containing group structures. The symmetric stretching vibration of the C–O–C bond between the oxygen and aromatic structure occurs at 1000–1400 cm<sup>-1</sup>. These structures in no. 1 and 2 coal account for 3.0 and 14.3%, respectively. The fitting peaks of no. 1 coal at 1115, 1137, and 1178 cm<sup>-1</sup>, and no. 2 coal at 1101 cm<sup>-1</sup> belong to the aliphatic ether functional group and C–O–C bond stretching vibration. The 1249 cm<sup>-1</sup> peak of no. 1 coal belongs to the antisymmetric stretching vibration of the C–O–C bond of the aromatic ether, and the peak area is 12.9%. The C–O bond of 1260–1330 cm<sup>-1</sup> is the stretching vibration inside the –COOH group with contents of no. 1 and 2 coal of

**Figure 5.** FTIR spectra of aliphatic hydrocarbon groups in coal. (a) no. 1 coal and (b) no. 2 coal.

2800–3000 cm<sup>-1</sup> band for quantitative analysis.<sup>48</sup> The wavenumber is methyl antisymmetric stretching vibration near 2940–2975 cm<sup>-1</sup> and methyl symmetric stretching vibration near 2865 ± 5 cm<sup>-1</sup>. The wavenumber of 2880–2940 cm<sup>-1</sup> represents the methylene antisymmetric stretching vibration, and the methylene symmetric stretching vibration occurs at ~2845 ± 10 cm<sup>-1</sup>. No. 1 coal showed the methyl group vibration at peaks of ~2943, 2962, and 2864 cm<sup>-1</sup>, and no. 2 coal also

showed a methyl vibration at  $\sim 2950$ ,  $2965$ , and  $2862\text{ cm}^{-1}$ , which accounted for 28.8 and 29.9%. No. 1 and 2 coal show mainly methylene antisymmetric stretching vibration, so coal contains more aliphatic chains or rings. The calculated areas of methyl and methylene are  $\sim 1:2.48$  and  $1:2.35$  in no. 1 and 2 coals, respectively.

**2.2. Model Construction.** The molecular composition of coal is centered on an aromatic nucleus, and many structural units with similar but different structures are connected by bridge bonds. There are also small molecular compounds.<sup>49</sup> The marginal atomic groups of the basic structural units of coal include carboxyl, phenolic hydroxyl, carbonyl, and methoxy groups with oxygen atoms, and alkyl branched side chains. The length of the molecular branch side chain is closely related to the rank of coal metamorphism. A deeper metamorphism yields a shorter side chain length and a smaller proportion of aliphatic group carbons and total carbons. When the carbon content is  $\sim 70\%$ , the alkyl carbon accounts for 8% of the total carbon, and the number of carbon atoms in the side chain is  $\sim 2-3$ . When the carbon content is  $\sim 80\%$ , alkyl carbon accounts for 6% of the total carbon with  $\sim 2.2$  carbon atoms. For an elemental carbon content of  $\sim 84\%$ , the number of alkyl carbon atoms is  $\sim 1.8$ . The main body of the coal structural unit is often expressed by parameters such as the number of condensed aromatic rings, the ratio of hydrogen to carbon atoms, the aromatic carbon rate, and the aromatic hydrogen rate. The bituminous coal with an 80% carbon content has two aromatic rings. A higher carbon content results in more rings. There are three aromatic rings in 85% coal. When the carbon content exceeds 90%, the coal structure may tend to graphitization or the number of closed rings exceeds 40. In addition to aromatic rings, nitrogen or sulfur atomic heterocycles may appear in the main structure. Bridge bonds occur at the connection between the molecular unit structures. The types of bridge bonds include  $-\text{CH}_2-$ methylene,  $-\text{O}-$ ,  $-\text{S}-$  iso-ether bonds, sulfide bonds,  $-\text{CH}_2-\text{O}-$ ,  $-\text{CH}_2-\text{S}-$  iso-methylene ether bonds, and methylene-sulfide bonds. The distribution quantity and position of bridge bonds in molecules differ, and the content is uneven. Low-rank bituminous coal is dominated by  $-\text{CH}_2-$  or  $-\text{CH}_2-\text{O}-$  groups, whereas medium metamorphic bituminous coal is dominated by  $-\text{O}-$  or  $-\text{CH}_2-$  in small quantities. As a vulnerable group of molecules, bridge bonds are prone to thermal or oxidative fracture, so bridge bonds reflect the stability of the coal molecular structure.

The parameters of the unit body are constructed through experimental data.

- (1) In the hydrogen carbon atom number ratio of the coal molecule,  $\text{H}/\text{C} = H_{\text{ad}}/(C_{\text{ad}}/12)$ ,  $H_{\text{ad}}$  and  $C_{\text{ad}}$  represent the hydrogen and carbon content of coal. The calculated  $\text{H}/\text{C}$  of no. 1 coal is 0.78 and that of no. 2 coal is 0.68.
- (2) Hydrogen atoms can be divided into aromatic and aliphatic hydrogen. The ratio of aromatic hydrogen to total hydrogen is the aromatic hydrogen rate  $f_{\text{ar}}^{\text{H}}$ , which is calculated using the FTIR peak region of aliphatic hydrocarbon radicals with wavenumbers in the band of  $2800-3000\text{ cm}^{-1}$  and aromatic substituted hydrogen in the band of  $700-900\text{ cm}^{-1}$ .  $f_{\text{ar}}^{\text{H}} = H_{\text{ar}}/H = I(675-900\text{ cm}^{-1})/[I(2800-3000\text{ cm}^{-1}) + I(675-900\text{ cm}^{-1})]$ , where  $I(A)$  represents the area of the A-band, and the calculated  $f_{\text{ar}}^{\text{H}}$  values of no. 1 and 2 coal are 0.25 and 0.41.
- (3) The properties of carbon atoms can be divided into aromatic and aliphatic. The ratio between the number of carbon atoms of the aromatic compounds and the total

carbon atoms is the aromatic carbon rate  $f_{\text{ar}} = 1 - C_{\text{al}}/C = 1 - [H_{\text{al}}/H^*(\text{H}/\text{C})]/(H_{\text{al}}/C_{\text{al}})$ , where  $C_{\text{al}}$  represents the amount of aliphatic carbon,  $C$  represents the total carbon,  $H_{\text{al}}$  is the amount of aliphatic hydrogen,  $H$  is the total hydrogen, and  $H_{\text{al}}/C_{\text{al}}$  is the number ratio of aliphatic hydrogen to carbon atoms, which is generally 1.8.<sup>50,51</sup> The  $f_{\text{ar}}$  of no. 1 coal is 0.68 and that of no. 2 coal is 0.78.

**Table 3. Atomic Number Ratios of Experimental Coal Samples**

coal sample	C:H:O:N:S
no. 1 coal	1:0.7832:0.1093:0.0156:0.0024
no. 2 coal	1:0.6799:0.0668:0.0173:0.0023

- (4) According to the percentage content of elements, the number of atoms that constitutes the coal structure is obtained, as shown in Table 3.

To facilitate calculation and simulation, the total number of carbon atoms of coal molecules is set to 60, and the basic structures of two bituminous coals are constructed. Therefore, theoretically, the molecular formulae of no. 1 and 2 coal are  $\text{C}_{60}\text{H}_{47}\text{O}_7\text{N}$  and  $\text{C}_{60}\text{H}_{40}\text{O}_4\text{N}$ .

The coal molecular difference shown in Table 4 is the absolute value of the difference between the simulated and experimental

**Table 4. Simulated Values and Differences of Coal Molecular Parameters**

characteristic parameter	simulated value of no. 1 coal	error value of no. 1 coal	simulated value of no. 2 coal	error value of no. 2 coal
C (%)	81.76	0.86	85.19	0.05
H (%)	5.54	0.26	5.26	0.43
O (%)	11.09	0.7	7.83	0.24
N (%)	1.62	0.15	1.71	0.01
H/C atomic number ratio	0.81	0.03	0.74	0.06
aromatic hydrogen rate $f_{\text{ar}}^{\text{H}}$	0.48	0.23	0.56	0.15
aromatic carbon rate $f_{\text{ar}}$	0.77	0.09	0.82	0.04

values, which shows the error in building the model. If sulfur atoms appear in the unit model, the error between the element content of coal molecules and the experimental value is large. To enhance the authenticity of the simulated structure, through infrared analysis and structural parameters, after continuous adjustment, optimization, and modification on the basis of previous work, the structural configuration plan of the no. 1 coal molecule is obtained, as shown in Figure 7a, and no. 2 coal is shown in Figure 7b (the spectral verification section is given in Section 2.4). The constructed molecular formulae are  $\text{C}_{59}\text{H}_{48}\text{O}_6\text{N}$  and  $\text{C}_{58}\text{H}_{43}\text{O}_4\text{N}$ . The aromatic hydrogen rate and the aromatic carbon rate of the simulated molecules are slightly higher than the experimental values. The errors of no. 1 and 2 coal are 0.23, 0.09, 0.15, and 0.04%, respectively.

**2.3. Simulation Verification of the Molecular Structure.** The COMPASSII force field is a molecular force field to unify the force field of organic molecular systems and that of inorganic molecular systems, which can be used to simulate

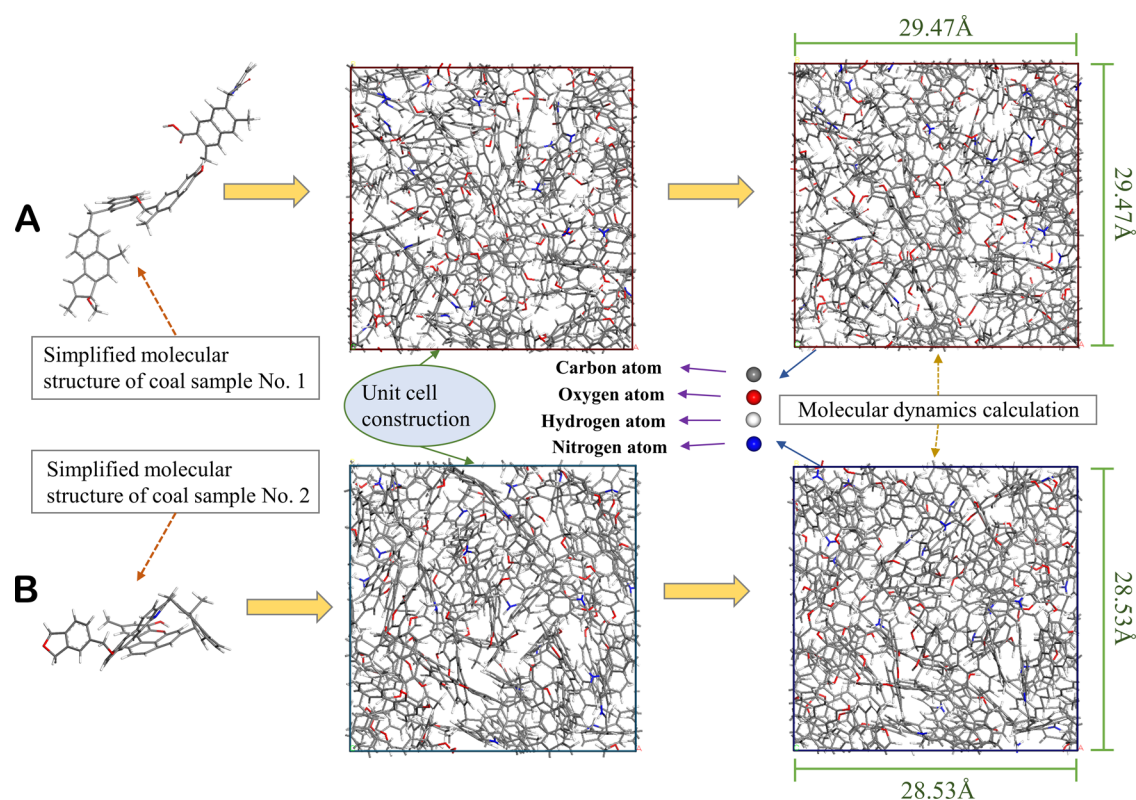


**Figure 6.** Construction of the bituminous coal molecular model. The upper part (A) is no. 1 coal. In the two boxes, the left is the geometrically optimized cell structure and the right is the cell structure calculated by molecular dynamics; the lower part (B) is no. 2 coal.

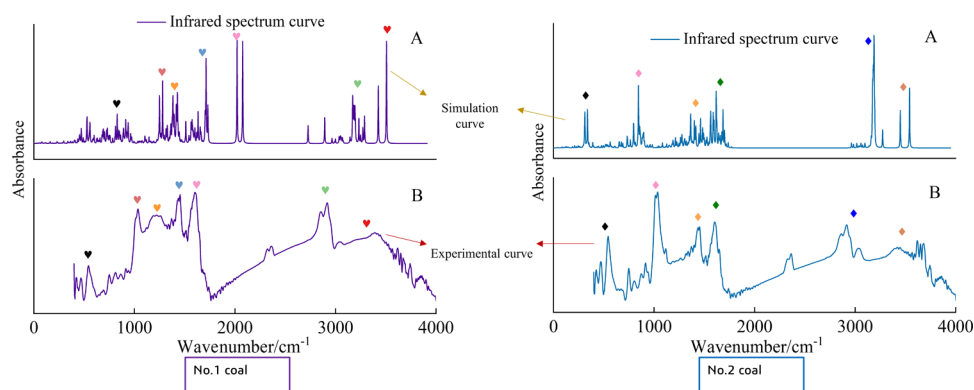


**Figure 7.** Calculation spectrum and the experimental spectrum. “A” represents the simulation curve and “B” represents the experimental curve.

organic and inorganic small molecules, polymers, some metal ions, etc. The force field parameters come from the empirical parameters of quantum mechanics calculated from ab initio. The COMPASSII force field can analyze and calculate the molecular structure, vibration frequency, conformational energy, crystal structure, and binding energy density of the system and analyze and predict isolated and condensed molecules’ structural energy characteristics.<sup>52</sup>

The structure at the lowest point of molecular structure energy has research significance. First, the structure of the coal molecular simplified model is optimized, the calculation is run using Materials Studio (MS) software, and the structure at the local energy minimum is optimized using force tools. The parameter settings are as follows: the force field is uniformly set to COMPASSII, and the maximum number of iterations is 5000. The first molecular dynamics simulation was carried out. The parameters are set as follows: the ensemble is NVT, the

temperature is 600.00 K, the control method is Nose, and the number of steps is 50000. To obtain a stable configuration, annealing dynamics simulation is required. The parameters are set as follows: annual, number of annual cycles is 5, initial temperature is 300.00 K, and mid-cycle temperature is 600.00 K. Finally, the second dynamic calculation is carried out, and the parameters are consistent with the first one. The calculation formula of molecular potential energy is given as follows<sup>53</sup>

$$E = E_V + E_N \quad (1)$$

$$E_V = E_B + E_A + E_T + E_I \quad (2)$$

$$E_N = E_{VAN} + E_E + E_H \quad (3)$$

where  $E_V$  is the valence electron energy, kcal/mol;  $E_N$  is the nonbonding energy, kcal/mol;  $E_B$  is the key stretching energy, kcal/mol;  $E_A$  is the bond angle energy, kcal/mol;  $E_T$  is the

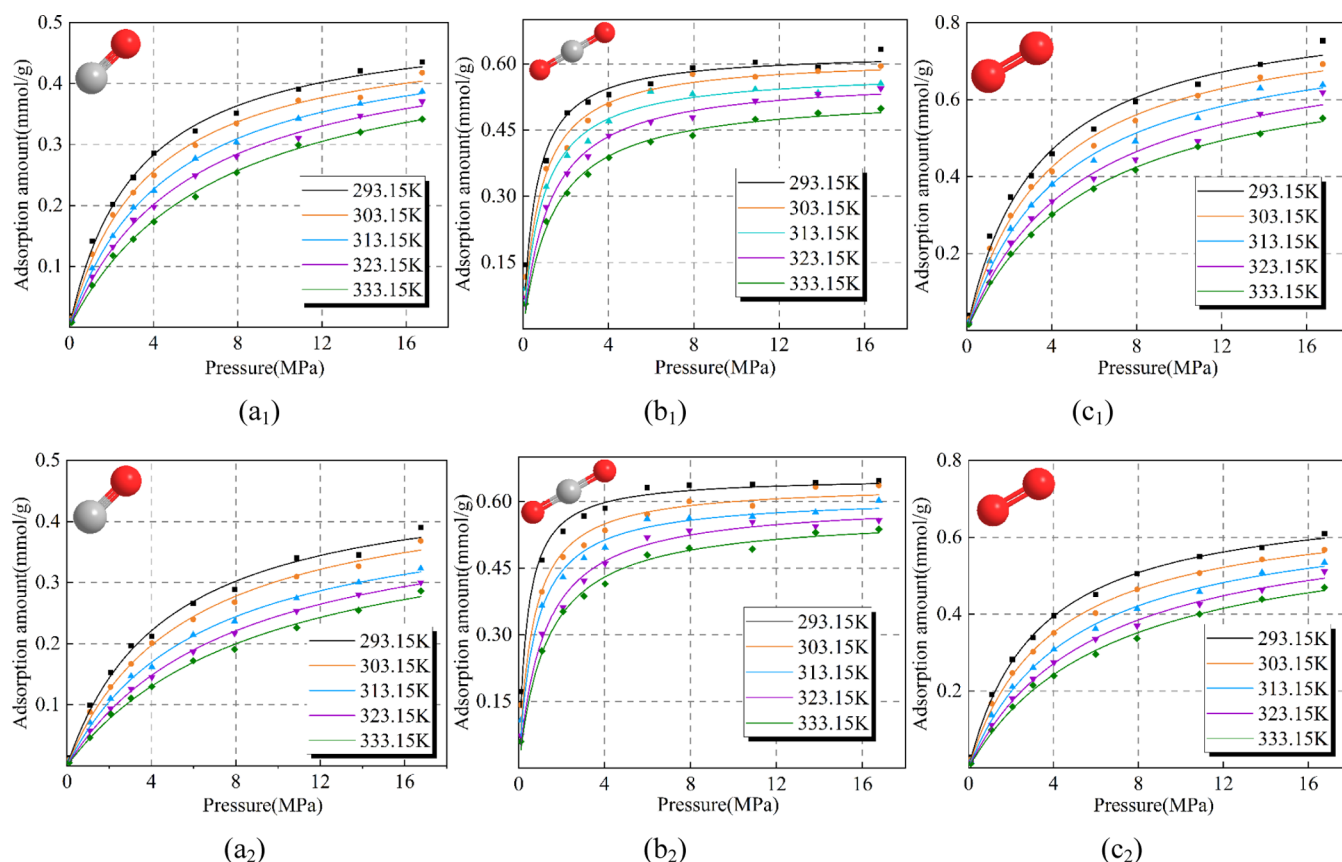


**Figure 8.** Isothermal adsorption curve of CO, CO<sub>2</sub>, and O<sub>2</sub> single-component gas. (a<sub>1</sub>) CO adsorption curve of no. 1 coal, (b<sub>1</sub>) CO<sub>2</sub> adsorption curve of no. 1 coal, and (c<sub>1</sub>) O<sub>2</sub> adsorption curve of no. 1 coal. (a<sub>2</sub>) CO adsorption curve of no. 2 coal, (b<sub>2</sub>) CO<sub>2</sub> adsorption curve of no. 2 coal, and (c<sub>2</sub>) O<sub>2</sub> adsorption curve of no. 2 coal.

torsional energy, kcal/mol;  $E_I$  is the inversion energy, kcal/mol;  $E_{VAN}$  is the van der Waals energy, kcal/mol;  $E_E$  is the Coulombic energy; and  $E_H$  is the hydrogen bond energy, kcal/mol.

After calculation, the molecular spatial structure of no. 1 and no. 2 coal is shown in Figure 6. The gray, white, red, and blue balls are carbon, hydrogen, oxygen, and nitrogen. The spatial structure of the coal molecules deformed and twisted at the bridge bond position. In no. 1 coal, the pyrrole structure is perpendicular to the aromatic ring in space, and a large angle torsion existed in the oxygen-containing functional group. An approximate vertical state exists between the aromatic ring of the no. 2 coal and the adjacent aromatic ring, the rotation range at the aliphatic group is large, and the spatial voids become more obvious. According to formulae (1), (2), and (3), the total molecular energy decreases significantly from 845.8 kcal/mol in the first dynamic simulation to 766.2 kcal/mol in the second simulation, indicating that the molecular structure tends to be stable, and  $E_B$  decreases from 93.4 to 78.8 kcal/mol. The stretching range of the bond becomes narrower,  $E_A$  decreases from 140.7 to 106.4 kcal/mol,  $E_{VAN}$  decreases from 42.7 to 37.0 kcal/mol, the bond angle is relatively contracted, and the molecular spacing becomes smaller.

The structure with the lowest energy is imported into the VAMP calculator in MS, the AM1 semiempirical Hamiltonian function in neglect of a diatomic differential overlap (NDDO) is used for geometric optimization, the calculation attribute is set to frequency, and the simulated infrared spectrum is obtained. In Figure 7, A is the infrared spectrum curve of the simulated molecules and B is the experimental infrared spectrum. The peak

shape of the simulation results is consistent with the experimental results with a slight difference in the peak position. Some simulated peak positions are close to the experimental peak positions. For example, the peak group at the aromatic ring-substitution position of no. 1 coal is caused by the bending vibration outside the  $-CH-$  bond plane. As another example, the peak group at 1000–1800  $\text{cm}^{-1}$  of the no. 2 coal spectrum that is caused by stretching or bending vibration of oxygen-containing functional groups simulated that the peak position deviation is small. The position of absorption peak A in no. 1 coal is slightly higher than that of B, with a quantity of  $\sim 170$  units. The peak position after translation is consistent with the experimental spectrum. B has a wide peak at  $\sim 3400 \text{ cm}^{-1}$ , and the peak shape of the calculated spectrum is sharp. The characteristic frequency of the group in the infrared spectrum shows a self-associated hydroxyl hydrogen bond region, which exhibits mainly an intermolecular force. A shows the infrared spectrum of only one molecule, and the hydrogen bond in the molecule is weak. Therefore, the peak is shown in the infrared spectrum, and the peak width accounts for a relatively narrow proportion of the total spectrum width. The situation of no. 1 and 2 coal at  $\sim 3400 \text{ cm}^{-1}$  is basically the same, and a single molecule results in the simulation with a peak at the same position. The simulated peaks of no. 2 coal at 1050, 1400, and 1600  $\text{cm}^{-1}$  are basically consistent with the experimental peaks. Excluding the influence of error and intermolecular force, the simulation results are satisfactory, which indicates that the structural unit is reasonable.<sup>54</sup>

Table 5. Langmuir Fitting Parameters of Single-Component Gas Adsorption

gas	temperature (K)	no. 1 coal			no. 2 coal		
		<i>a</i> (mmol/g)	<i>b</i> (1/MPa)	<i>R</i> <sup>2</sup>	<i>a</i> (mmol/g)	<i>b</i> (1/MPa)	<i>R</i> <sup>2</sup>
CO	293.15	0.5089	0.3137	0.9961	0.4770	0.2163	0.9922
	303.15	0.4930	0.2710	0.9955	0.4695	0.1813	0.9947
	313.15	0.4901	0.2152	0.9993	0.4376	0.1581	0.9972
	323.15	0.4854	0.1776	0.9978	0.4367	0.1282	0.9990
	333.15	0.4851	0.1413	0.9980	0.4281	0.1094	0.9960
CO <sub>2</sub>	293.15	0.6268	1.6564	0.9697	0.6551	2.5980	0.9836
	303.15	0.6145	1.2373	0.9758	0.6389	1.5385	0.9698
	313.15	0.5841	1.0949	0.9816	0.6113	1.3102	0.9835
	323.15	0.5713	0.7999	0.9905	0.6015	0.8550	0.9890
	333.15	0.5313	0.6946	0.9920	0.5712	0.7621	0.9923
O <sub>2</sub>	293.15	0.8565	0.3028	0.9884	0.7127	0.3102	0.9980
	303.15	0.8282	0.2625	0.9930	0.6873	0.2628	0.9973
	313.15	0.7959	0.2277	0.9925	0.6751	0.2082	0.9969
	323.15	0.7710	0.1899	0.9889	0.6647	0.1721	0.9964
	333.15	0.7291	0.1744	0.9988	0.6442	0.1510	0.9964

**2.4. Adsorption Simulation Design.** After the simplified molecular model is optimized, the amorphous cell module in MS adds periodic boundary conditions to the simplified model.<sup>21</sup> The structure is optimized until the total energy converges. The task is construction, the quality is fine, the density is 1.400 g/cm<sup>3</sup>, force field is COMPASSII, and the electrostatics is Ewald. After a series of geometric optimization and dynamic calculations, the system with the lowest energy is selected for subsequent calculation, the unit-cell size of the no. 1 coal is 2.947 × 2.947 × 2.947 nm (C<sub>1180</sub>H<sub>960</sub>O<sub>120</sub>N<sub>20</sub>), and the unit-cell volume of the no. 2 coal is 2.853 × 2.853 × 2.853 nm (C<sub>1160</sub>H<sub>860</sub>O<sub>80</sub>N<sub>20</sub>), as shown in Figure 6. It should be noted that the construction of periodic coal molecules does not represent the actual real molecules but only the statistical results of the distribution of main functional groups in coal. The simulated infrared spectrum shows that the chemical bond and composition in the model are consistent with the actual situation. Therefore, coal molecules with periodic boundary conditions can intuitively show the adsorption state of coal, which makes the simulation study easier to understand.<sup>55,56</sup>

Different temperatures and pressures corresponding to the geological burial depth are selected. The surface temperature is set at 20 °C; the temperature gradients are set at 30, 40, 50, and 60 °C; the surface pressure is 101 kPa, the burial depths are 0, 100, 200, 300, 400, 600, 800, 1100, 1400, and 1700 m, and the hydrostatic pressure gradient is 0.0098 MPa/m, so 100 m: 1081 kPa, 200 m: 2061 kPa 300 m: 3041 kPa, 400 m: 4021 kPa, 600 m: 5981 kPa, 800 m: 7941 kPa, 1100 m: 10881 kPa, 1400 m: 13,821 kPa, and 1700 m: 16,761 kPa.<sup>25</sup> The pressure is calculated at different burial depths under five temperature gradients of CO, CO<sub>2</sub>, and O<sub>2</sub> single gases. Then, the absolute adsorption capacity of mixed gas with CO ratios of 0.1, 0.3, 0.5, 0.7, and 0.9 is calculated. Isothermal adsorption curves are formed at different temperatures, and the adsorption differences of bituminous coal with different metamorphic degrees are compared. The competitive behavior of two bituminous coals under different pressures is judged by the adsorption competitive selectivity of CO and other gases.

The gas isothermal adsorption curve is calculated by the grand canonical Monte Carlo simulation method and realized by Materials Studio software sorption tools.<sup>57</sup> Task: fixed pressure, quality: ultrafine, and force field: COMPASSII. The conversion between fugacity and pressure is converted by the Peng

Robinson formula,<sup>23</sup> in which fugacity is directly proportional to pressure.

Through the calculation of competitive adsorption energy by the Sorption module in MS software, the adsorption position and state of the adsorbate gas molecules in the model can also be observed, and the adsorption characteristics can be further clarified. Specific simulation parameter settings are as follows: task: locate, Monte Carlo method: Metropolis, force field: COMPASSII, and charges: force field assigned. The temperature was set to 293.15 K and the pressure to 8 MPa.

### 3. RESULTS AND DISCUSSION

**3.1. Single-Component Gas Adsorption of CO, O<sub>2</sub>, and CO<sub>2</sub>.** The single-component gas adsorption curves of the no. 1 coal and no. 2 coal are shown in Figure 8. The adsorption curves of CO, CO<sub>2</sub>, and O<sub>2</sub> of no. 1 coal are expressed by (*a*<sub>1</sub>), (*b*<sub>1</sub>), and (*c*<sub>1</sub>), respectively. The adsorption curves of no. 2 coal are (*a*<sub>2</sub>), (*b*<sub>2</sub>), and (*c*<sub>2</sub>). The fitting results of the adsorption curves in Figure 8 comply with the Langmuir equation,<sup>58</sup> and the Langmuir fitting formula is given as follows:

$$y = \frac{abx}{1 + bx} \quad (4)$$

where *a* represents the saturated adsorption capacity at infinite pressure, mmol/g; *b* is the adsorption constant, MPa<sup>−1</sup>; and *R*<sup>2</sup> is the fitting degree. The closer the value of *R*<sup>2</sup> is to 1, the closer the fitting degree is to the real value. The parameter values are shown in Table 5.

Under the same pressure, the adsorption capacity of both coal samples decreases with increasing temperature. The no. 1 coal generally has more significant adsorption capacity for CO and O<sub>2</sub> than the no. 2 coal under identical temperature and pressure. Because the rank of no. 1 coal metamorphism is low, the molecular structure is loose, many functional diagrams easily participate in the oxidation reaction, and the occurrence probability of CO and O<sub>2</sub> near the short-chain alkane structure becomes greater. CO is the product of the coal oxygen reaction and the oxide involved in the oxidation reaction. Compared with coal, which is not easy to oxidize, CO more easily exists in the structure of easily oxidized coal through molecular gaps. The adsorption between CO<sub>2</sub> and coal molecules occurs mainly through dispersion force, and an increase in the number of condensation rings leads to an increase in adsorption potential.

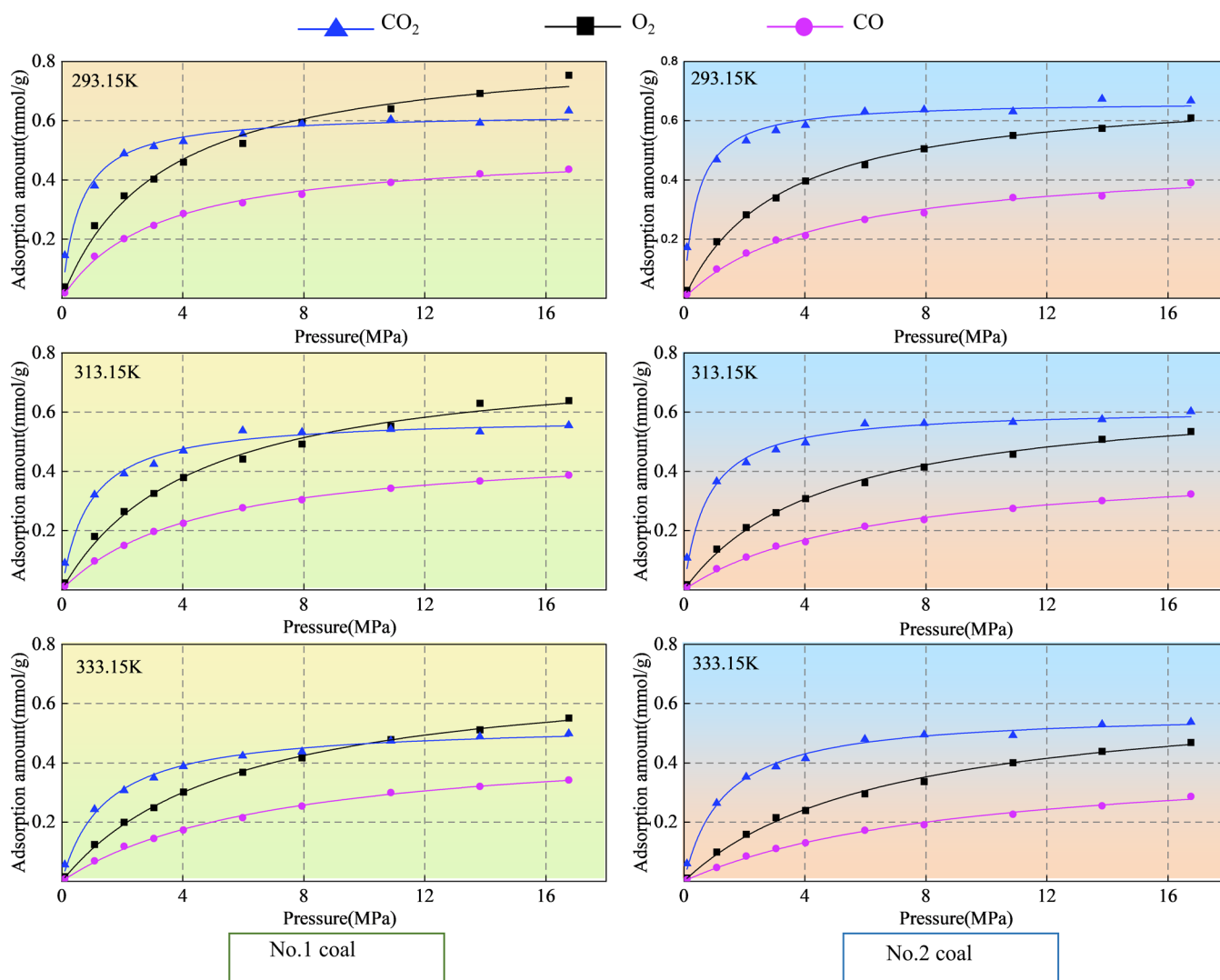


Figure 9. Adsorption capacity of the single-component gas.

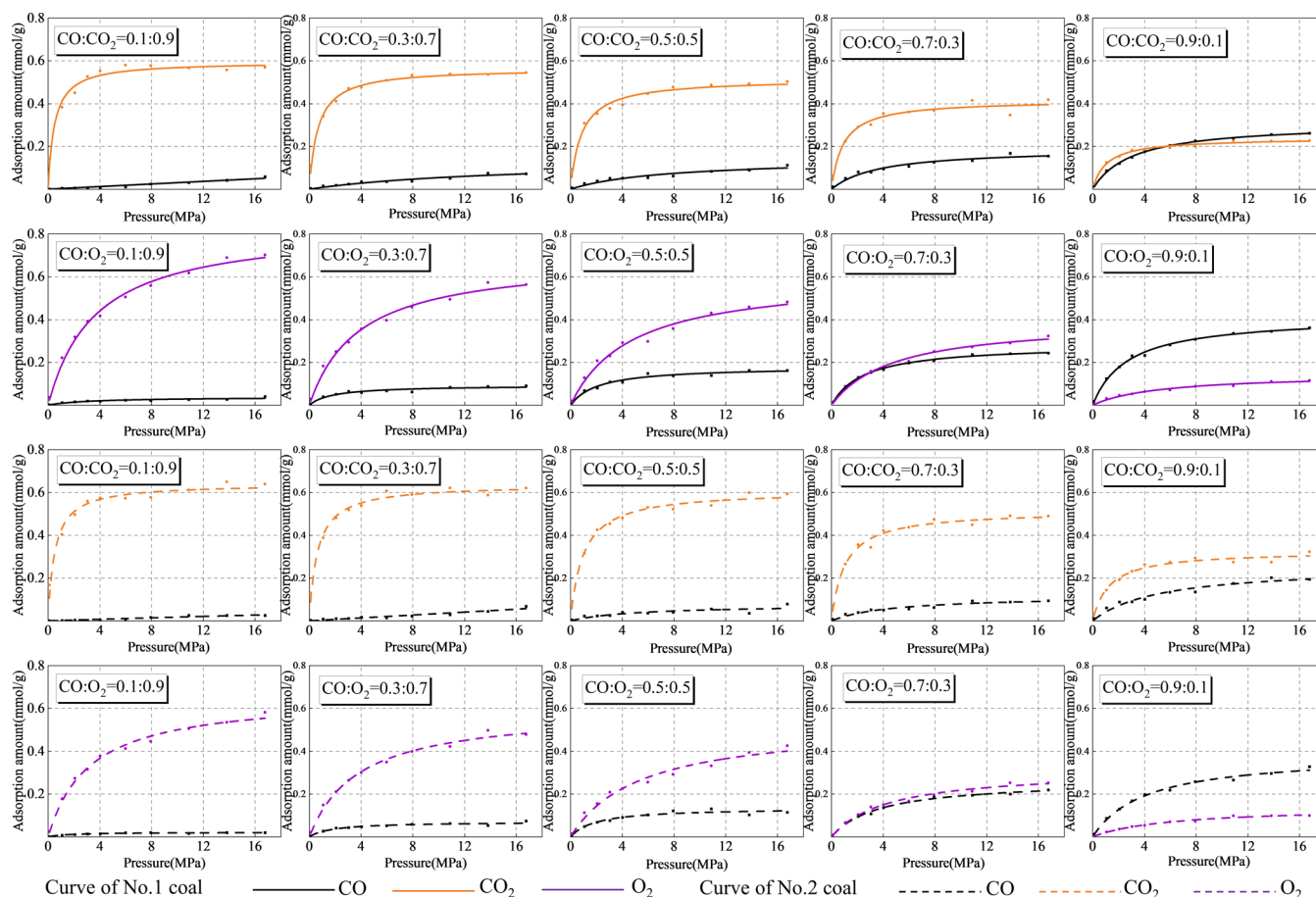
Therefore, the adsorption capacity of  $\text{CO}_2$  is stronger in coal molecules with a higher coalification degree.<sup>59</sup>

Figure 9 shows the variation curve of the single-component gas adsorption capacity of two coal samples with pressure at the same temperature. The adsorption capacity is related to the physical properties of individual molecules and other factors. The no. 2 coal sample has the highest  $\text{CO}_2$  adsorption capacity, which is greater than the CO and  $\text{O}_2$  adsorption capacity. Higher critical temperature and pressure correspond to greater adsorption capacity.<sup>60</sup> The no. 1 coal has the largest  $\text{CO}_2$  adsorption capacity in the range of 0–6.5 MPa. The adsorption law is that a larger molecular dynamics diameter corresponds to a smaller adsorption capacity.<sup>24</sup> The saturated adsorption pressure of  $\text{CO}_2$  is approximately 8 MPa, which is significantly lower than  $\text{O}_2$  and CO. The  $\text{CO}_2$  and  $\text{O}_2$  adsorption capacity cross point moves backward with increasing temperature. After the crossing point, the adsorption capacity of  $\text{O}_2$  significantly increases, which may be caused by the smallest molecular dynamics diameter of  $\text{CO}_2$ .  $\text{O}_2$  continues to occupy the adsorption site after it first tends to saturate. A deeper coal seam experiences a greater pressure, which is not conducive to gas adsorption. When the burial depth is less than approximately 650 m,  $\text{CO}_2$  injection should be used to prevent the coal seam oxygen concentration from being too high and prevent the

physical adsorption of oxygen from further transforming into a coal oxygen chemical reaction.<sup>61</sup> Figure 9 shows that the adsorption capacity of  $\text{CO}_2$  and  $\text{O}_2$  is much greater than that of CO.

**3.2. Binary Competitive Adsorption of CO with  $\text{O}_2$  and  $\text{CO}_2$ .** In Figure 10, the solid line represents the adsorption curves of CO,  $\text{O}_2$ , and  $\text{CO}_2$  of no. 1 coal at 293.15 K; and the molar ratios are 0.1:0.9, 0.3:0.7, 0.5:0.5, 0.7:0.3, and 0.9:0.1. Figure 10 represents the adsorption curve of no. 2 coal.

Figure 10 shows an apparent correlation between the number of small molecules adsorbed by the crystal cell and the molar ratio, and there is a general law in direct proportion. For no. 1 coal, the  $\text{CO}_2$  adsorption capacity rapidly increases in the stage of 0–4 MPa, and the adsorption capacity tends to be flat after 8 MPa. The rapid growth stage of CO is at 0–8 MPa. Obviously, in the competitive adsorption of  $\text{CO}_2$  and CO, the low-pressure stage can be close to the saturation state. When the molar ratio of CO is much greater than that of  $\text{CO}_2$ , the adsorption capacity of CO and  $\text{CO}_2$  is approximately 6 MPa. When the molar ratio of CO to  $\text{CO}_2$  in the coal seam is less than 0.7:0.3,  $\text{CO}_2$  injection can be used for fire prevention.<sup>52</sup> However, when the molar ratio of CO is approximately 9 times that of  $\text{CO}_2$ , the effect of the  $\text{CO}_2$  injection fire prevention technology is not significant. With increasing buried depth pressure, the effect is less obvious. In



**Figure 10.** Competitive adsorption curve of CO, CO<sub>2</sub>, and O<sub>2</sub>. The solid line represents no. 1 coal and the dotted line represents no. 2 coal.

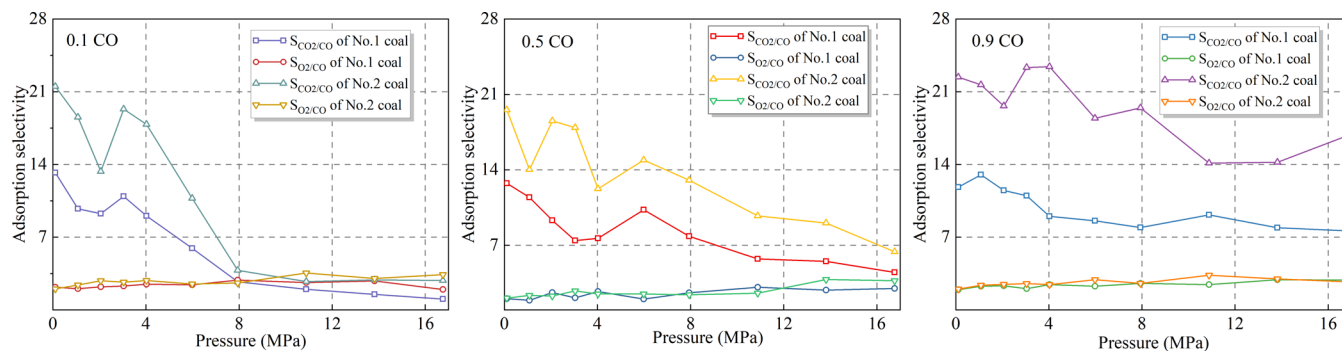


**Figure 11.** Competitive adsorption selectivity: (a) 10% CO, (b) 50% CO, and (c) 90% CO.

terms of the competitive adsorption capacity of different molar ratios of CO and O<sub>2</sub>, when the molar ratio of CO to O<sub>2</sub> is small or 1, the adsorption capacity of O<sub>2</sub> is higher than that of CO. The adsorption capacity is close at 0.7:0.3 and 0.9:0.1, and the adsorption capacity of CO is better than that of O<sub>2</sub>. As a polar molecule, CO will inhibit the adsorption of O<sub>2</sub> when CO occupies a high molar ratio. When the adsorption capacity of O<sub>2</sub> is higher than that of CO, air leakage should be controlled to prevent CO in coal seams containing primary CO from desorbing to improve the accuracy of predicting spontaneous coal combustion when CO is used as the index gas.<sup>40</sup>

For no. 2 coal, compared with the CO<sub>2</sub> competitive adsorption capacity, the stronger adsorption capacity is shown by CO<sub>2</sub>. With increasing CO molar ratio, the CO adsorption capacity also increases. The decrease in CO<sub>2</sub> adsorption is more

significant than CO adsorption. Changing the molar ratio significantly affects the adsorption capacity of CO<sub>2</sub>, so a high proportion of CO<sub>2</sub> will affect the adsorption capacity of CO. The CO<sub>2</sub> adsorption capacity of no. 2 coal at any molar ratio is stronger than that of no. 1 coal under identical conditions, which is consistent with the conclusion of single-gas adsorption. The change law of the competitive adsorption of CO and O<sub>2</sub> is consistent with that of the no. 1 coal. At 0.7:0.3, the isothermal adsorption curves of CO and O<sub>2</sub> at 0–4 MPa are close to coincidence, which indicates that in this case, the ability of CO and O<sub>2</sub> to occupy the adsorption site is equivalent. With increasing burial depth pressure, the CO adsorption capacity is slightly less than the O<sub>2</sub> adsorption capacity. Even if the oxygen concentration is small, the oxidation reaction of coal remains.<sup>62</sup> Therefore, when the spontaneous combustion of the coal

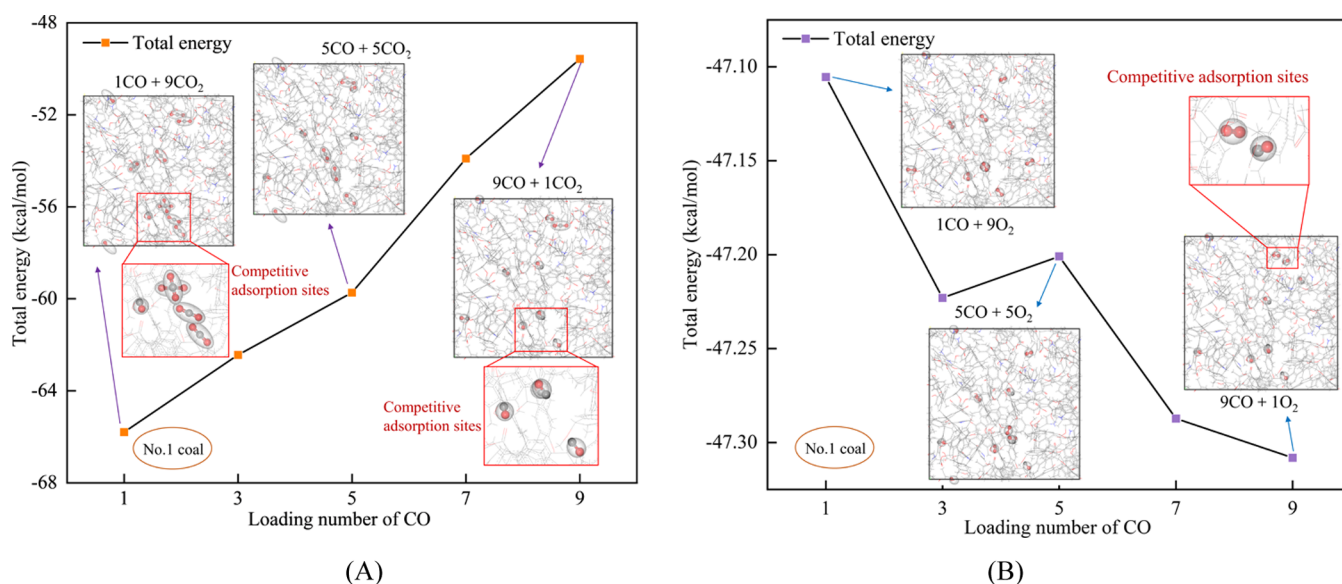


**Figure 12.** Competitive adsorption sites of no. 1 coal. (A) Energy and adsorption site changes of CO and CO<sub>2</sub> and (B) CO and O<sub>2</sub>.

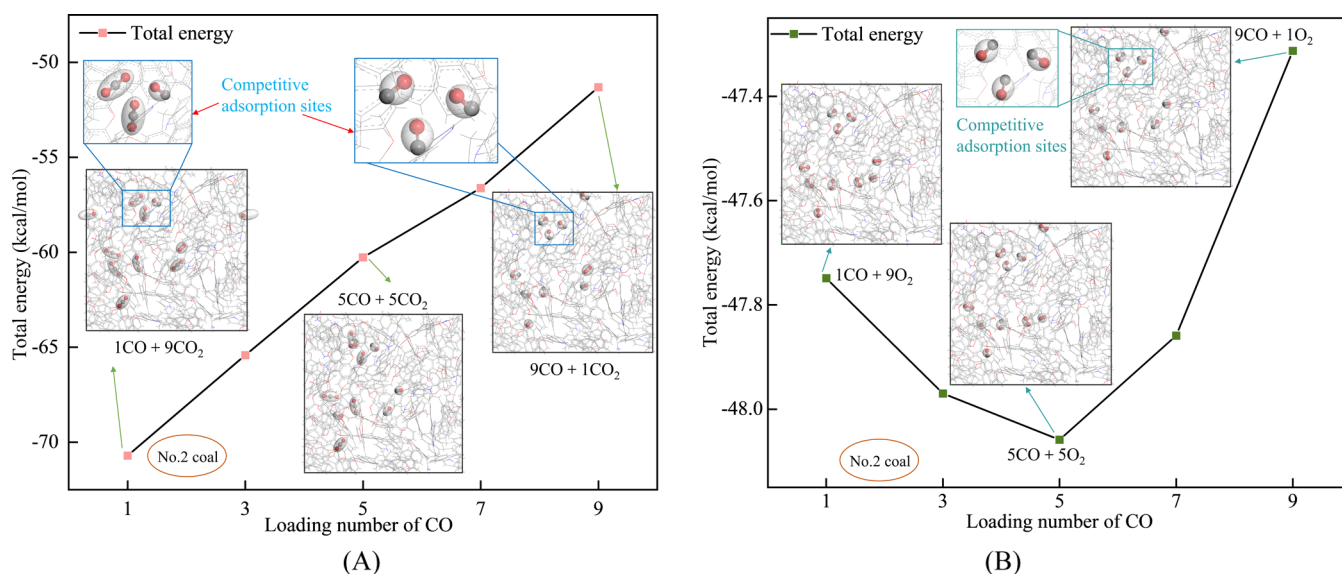


**Figure 13.** Competitive adsorption sites of no. 2 coal. (A) Energy and adsorption site changes of CO and CO<sub>2</sub> and (B) CO and O<sub>2</sub>.

oxygen reaction occurs, oxygen is consumed for a short time, which rapidly decreases the oxygen concentration, and the CO concentration, which is the product of the coal oxygen reaction, increases. The CO adsorption index actively changes with the decrease in oxygen, so it can respond to the degree of the coal oxidation reaction.

**3.3. Adsorption Selectivity of CO.** Adsorption selectivity refers to the ability of adsorbents to preferentially adsorb some substances due to their different components and structures. The adsorption selectivity of binary mixtures of other gases G and CO is defined as

$$S_{G/CO} = \frac{x_G/x_{CO}}{y_G/y_{CO}} \quad (5)$$

where  $x_G$  is the mole fraction of gas G in the adsorption component,  $x_{CO}$  is the mole fraction of CO in the adsorption component, and  $y_G$  and  $y_{CO}$  are the mole fractions of G and CO in the free state. When  $S_{G/CO}$  is greater than 1, in the binary

mixed gas, G is preferentially adsorbed by the adsorbent compared with CO, and the adsorption capacity of the adsorbent for G is stronger. G is easily enriched in the adsorbent.<sup>63</sup>

Figure 11a,c shows the difference in adsorption selectivity between CO, CO<sub>2</sub>, and O<sub>2</sub> at 293.15 K. The adsorption selectivity of CO<sub>2</sub>/CO decreases with increasing pressure, and the competitiveness of CO relative to CO<sub>2</sub> increases. When the CO concentration is 0.1, the changing trend of the ordinate corresponding to 0~17 MPa is the largest, and the decrease range of adsorption selectivity at 0.5 CO is less than that of 0.1 CO. At 0.9 CO, the downward trend is gradually gentle, both coal samples have an evident gentle trend with the increase in the amount and concentration of CO, and the competitive selectivity of CO increases. However,  $S_{CO_2/CO}$  remains greater than 1, and CO<sub>2</sub> remains significantly more competitive than CO, which is consistent with the conclusion of their binary adsorption curves. When the pressure is less than 8 MPa, the

adsorption selectivity values of the two coal samples fluctuate in a certain range. After 8 MPa, the adsorption selectivity of CO<sub>2</sub>/CO is significantly inhibited, and it is evident at 0.1 CO. When the CO concentration is low, the competitiveness after 8 MPa is considerably more substantial than that before 8 MPa.

Coal with a high coal mineralization degree showed a greater adsorption selectivity for CO<sub>2</sub>/CO, and the adsorption selectivity increased when the amount of CO species increased. The selectivity for O<sub>2</sub>/CO shows a slightly increasing trend. All competitive adsorption capacities of O<sub>2</sub> are larger than those of CO at different species concentrations.<sup>64</sup> Adsorption selectivity for O<sub>2</sub>/CO:  $S_{O_2/CO} > S_{CO_2/CO}$  at pressures greater than 8 MPa in 0.1 CO.

### 3.4. Competitive Adsorption Energy of the Adsorbate.

There are 10 adsorbate gas molecules, and the number of CO molecules is set to 1, 3, 5, 7, and 9. Correspondingly, the number of CO<sub>2</sub> is set to 9, 7, 5, 3, and 1. The number of O<sub>2</sub> is equal to that of CO<sub>2</sub>. Figure 12A shows the total energy change of CO and CO<sub>2</sub> competitive adsorption in the no. 1 coal. The adsorption process is an exothermic process. In the competition between CO and CO<sub>2</sub>, the CO amount is positively correlated with the total energy. The nonbonding energy accounts for the major part of the total energy, while the van der Waals energy accounts for the major part of the nonbonding energy. The van der Waals energy is consistent with the changing trend of the total energy and is positively correlated with the number of CO atoms. At 1CO + 9CO<sub>2</sub>, the nonbond energy is −71.34 kcal/mol, and the van der Waals energy is −59.78 kcal/mol. At 5CO + 5CO<sub>2</sub>, the van der Waals energy is −51.99 kcal/mol. At 9CO + 1CO<sub>2</sub>, the van der Waals energy is −47.77 kcal/mol. Therefore, most adsorption occurs due to van der Waals energy. The adsorption energies of CO and O<sub>2</sub> are also mainly dependent on the van der Waals energy. Although the curve in Figure 12B shows an overall downward trend, the difference between the lowest energy and the highest energy is only approximately 0.20 kcal/mol. The increase in the CO amount did not greatly change the total energy. Figure 13A shows the competitive adsorption energy of CO and CO<sub>2</sub> in the no. 2 coal, and the changing trend is basically identical to that of the no. 1 coal. The total energy significantly changes with the change in the amount of CO and CO<sub>2</sub>. In Figure 13B, the total energy of CO and O<sub>2</sub> competitive adsorption slightly fluctuates. Figures 12 and 13 clearly show that the angle, aggregation, and dispersion of the adsorbate change and the quantity and the concentration of the adsorbate also affect the variation in adsorption sites. The total energy can reflect the stability of the system's equilibrium state. All systems tend to decrease in energy. A greater absolute value of the total energy corresponds to a greater decrease in energy, i.e., adsorption will more likely occur in a more stable system.<sup>20</sup> Therefore, in the competition between CO and CO<sub>2</sub>, more CO<sub>2</sub> makes the system more stable. In other words, the increase in molarity of CO will increase the instability of the system. The total energy of the mixed system containing CO and O<sub>2</sub> has no significant difference, and the energy difference has no obvious rule with the change in the adsorbent molar concentration. However, the no. 2 coal has a larger total energy than the no. 1 coal, so the competitive adsorption of CO and O<sub>2</sub> may be greatly affected by the coal structure itself.

## 4. CONCLUSIONS

- (1) The structures of two bituminous coal molecules were constructed by FTIR experiments. The molecular

formulae of the no. 1 and no. 2 coals are C<sub>1180</sub>H<sub>960</sub>O<sub>120</sub>N<sub>20</sub> and C<sub>1160</sub>H<sub>860</sub>O<sub>80</sub>N<sub>20</sub>, respectively. The simulation infrared spectra verify that the construction model is reasonable.

- (2) For the adsorption of a single-component gas, within the temperature change of 293.15–333.15 K, the adsorption capacity of CO, CO<sub>2</sub>, and O<sub>2</sub> increased with increasing pressure and gradually reached saturation. The fitting curve is consistent with the isothermal adsorption Langmuir equation. Under an identical buried depth pressure, the increase in temperature will inhibit the adsorption capacity of a single-component gas, which shows a negative correlation between temperature and adsorption capacity. When the temperature is 20 °C and the pressure is less than 6.5 MPa, the adsorption capacity is CO<sub>2</sub> > O<sub>2</sub> > CO. The pressure when CO<sub>2</sub> reaches saturated adsorption is smaller than that of CO and O<sub>2</sub>.
- (3) In binary competitive adsorption, the adsorption curves of 90% CO and 10% CO<sub>2</sub> are close, and the adsorption capacity of CO<sub>2</sub> is significantly inhibited with increasing CO concentration. A higher coalification degree of bituminous coal corresponds to a greater adsorption selectivity of CO<sub>2</sub>/CO. The adsorption capacity between 70% CO and 30% O<sub>2</sub> is close. When CO is higher than 70%, CO has greater adsorption competitiveness than O<sub>2</sub>. Therefore, when the CO content of the original coal seam is high or CO anomalies occur underground, it is not suitable to reduce the CO adsorption by injecting gas. For coal seam fire prevention, grouting or other methods should be changed to control the air leakage of the working face, prevent excessive O<sub>2</sub> from occupying the adsorption site, coal from further spontaneous combustion, and CO adsorbed by coal from diffusing and seeping into the working face.

## AUTHOR INFORMATION

### Corresponding Author

Xianwei Dong – College of Mining Engineering, North China University of Science and Technology, Tangshan 063210, China; Mining Development and Safety Technology Key Lab of Hebei Province, Tangshan 063210, China; [orcid.org/0000-0001-7029-4081](https://orcid.org/0000-0001-7029-4081); Email: [dxw0327@163.com](mailto:dxw0327@163.com)

### Authors

Xuanmeng Dong – College of Mining Engineering, North China University of Science and Technology, Tangshan 063210, China

Fusheng Wang – College of Mining Engineering, North China University of Science and Technology, Tangshan 063210, China; Mining Development and Safety Technology Key Lab of Hebei Province, Tangshan 063210, China; [orcid.org/0000-0002-2950-7927](https://orcid.org/0000-0002-2950-7927)

Liwen Guo – College of Mining Engineering, North China University of Science and Technology, Tangshan 063210, China; Mining Development and Safety Technology Key Lab of Hebei Province, Tangshan 063210, China

Yu Zhang – College of Mining Engineering, North China University of Science and Technology, Tangshan 063210, China; Mining Development and Safety Technology Key Lab of Hebei Province, Tangshan 063210, China; [orcid.org/0000-0002-2638-6285](https://orcid.org/0000-0002-2638-6285)

Complete contact information is available at:

<https://pubs.acs.org/10.1021/acsomega.2c00831>

## Notes

The authors declare no competing financial interest.

## ACKNOWLEDGMENTS

This research was conducted with financial support from the National Natural Science Foundation of China (grant no. 51974128).

## REFERENCES

- (1) Xia, W.; Xie, G.; Peng, Y. Recent advances in beneficiation for low rank coals. *Powder Technol.* **2015**, *277*, 206–221.
- (2) Dutta, S. N.; Dowerah, D.; Frost, D. C. J. F. Study of sulphur in Assam coals by X-ray photoelectron spectroscopy. *Fuel* **1983**, *62*, 840–841.
- (3) Jing, Z.; Rodrigues, S.; Strounina, E.; Li, M.; Wood, B.; Underschultz, J. R.; Esterle, J. S.; Steel, K. M. Use of FTIR, XPS, NMR to characterize oxidative effects of NaClO on coal molecular structures. *Int. J. Coal Geol.* **2019**, *201*, 1–13.
- (4) Qin, Z. New advances in coal structure model. *Int. J. Min. Sci. Technol.* **2018**, *28*, 541–559.
- (5) Moore, T. A. Coalbed methane: A review. *Int. J. Coal Geol.* **2012**, *101*, 36–81.
- (6) Chen, C.; Gao, J.; Yan, Y. Observation of the type of hydrogen bonds in coal by FTIR. *Energy Fuels* **1998**, *12*, 446–449.
- (7) Chen, Y.; Mastalerz, M.; Schimmelmann, A. Characterization of chemical functional groups in macerals across different coal ranks via micro-FTIR spectroscopy. *Int. J. Coal Geol.* **2012**, *104*, 22–33.
- (8) Solomon, P. R.; Carangelo, R. M. FTIR analysis of coal. 1. techniques and determination of hydroxyl concentrations. *Fuel* **1982**, *61*, 663–669.
- (9) He, L.; Lin, Q.; Liu, Y.; Huang, Y. Unique catalysis of Ni-Al hydrotalcite derived catalyst in CO<sub>2</sub> methanation: cooperative effect between Ni nanoparticles and a basic support. *J. Energy Chem.* **2014**, *23*, 587–592.
- (10) Liu, Y.; Jennifer, W. CO<sub>2</sub> adsorption on carbon models of organic constituents of gas shale and coal. *Environ. Sci. Technol.* **2011**, *45*, 809–814.
- (11) Shi, X.; Zhang, Y.; Chen, X.; Zhang, Y. J. F. Effects of thermal boundary conditions on spontaneous combustion of coal under temperature-programmed conditions. *Fuel* **2021**, *295*, No. 120591.
- (12) Shi, X.; Zhang, Y.; Chen, X.; Zhang, Y.; Rui, L.; Guo, R.; Zhao, T.; Deng, Y. Numerical simulation on response characteristics of coal ignition under the disturbance of fluctuating heat. *Combust. Flame* **2022**, *237*, No. 111870.
- (13) Karsner, G. G.; Perlmutter, D. D. J. F. Model for coal oxidation kinetics. 1. Reaction under chemical control. *Fuel* **1982**, *61*, 29–34.
- (14) Fang, X.; Yao, H. *Experimental Study on the Displacement of Oxygen in Coal with Different Particle Sizes by Inert Gas*; Industry and Mine Automation, 2021; Vol. 47, pp 101–107.
- (15) Li, S. *Research on Low-Temperature Oxidation Characteristics of Coalbased on Physical Factors*; Tianjin University of Technology: Tianjin, 2021; pp 20–36.
- (16) Chen, L.; Lu, C.; Yu, M.; Lin, M.; Jia, H. Study on oxygen physisorption of coal at low temperature and the influence of moisture. *Energy Technol. Manage.* **2008**, *5*, 88–90.
- (17) Lu, J.; He, Y.; Cheng, G. Construction of Lignite Macromolecular Model and its Analysis on Physisorption Oxygen at Low Temperatures. *Min. Res. Dev.* **2021**, *41*, 58–66.
- (18) Cheng, G.; Li, Y.; Zhang, M.; Cao, Y. Simulation of the adsorption behavior of CO<sub>2</sub>/N<sub>2</sub>/O<sub>2</sub> and H<sub>2</sub>O molecules in lignite. *J. China Coal Soc.* **2021**, No. 673.
- (19) Xue, D.; Hu, X.; Cheng, W.; Wu, M.; Shao, Z.; Yla, B.; Zhao, Y.; Zhang, K. Carbon dioxide sealing-based inhibition of coal spontaneous combustion: A temperature-sensitive micro-encapsulated fire-retardant foamed gel. *Fuel* **2020**, *266*, No. 117036.
- (20) Wu, S.; Deng, C.; Dai, F.; Gao, F.; Wang, X. Differences of ability and competitiveness on coal adsorbing CO<sub>2</sub>, O<sub>2</sub> and N<sub>2</sub>. *Chin. J. Environ. Eng.* **2017**, *11*, 4229–4235.
- (21) Zhou, W.; Wang, H.; Zhang, Z.; Chen, H.; Liu, X. J. R. A. Molecular simulation of CO<sub>2</sub>/CH<sub>4</sub>/H<sub>2</sub>O competitive adsorption and diffusion in brown coal. *RSC Adv.* **2019**, *9*, 3004–3011.
- (22) Zhou, W.; Wang, H.; Yan, Y.; Liu, X. Adsorption Mechanism of CO<sub>2</sub>/CH<sub>4</sub> in Kaolinite Clay: Insight from Molecular Simulation. *Energy Fuels* **2019**, *33*, 6542–6551.
- (23) Gao, D.; Hong, L.; Wang, J.; Zheng, D. Molecular simulation of gas adsorption characteristics and diffusion in micropores of lignite. *Fuel* **2020**, *269*, No. 117443.
- (24) Wang, X.; Zhai, Z.; Jin, X.; Wu, S.; Li, J.; Sun, L.; Liu, X. Molecular simulation of CO<sub>2</sub>/CH<sub>4</sub> competitive adsorption in organic matter pores in shale under certain geological conditions. *Pet. Explor. Dev. t* **2016**, *43*, 841–848.
- (25) Zhang, J.; Liu, K.; Clennell, M. B.; Dewhurst, D. N.; Pervukhina, M. Molecular simulation of CO<sub>2</sub>–CH<sub>4</sub> competitive adsorption and induced coal swelling. *Fuel* **2015**, *160*, 309–317.
- (26) Ding, Y. *Research on the Mechanism of CH<sub>4</sub>/CO<sub>2</sub>/H<sub>2</sub>O and O<sub>2</sub> Adsorption on Coal Molecule*; North China Electric Power University: Baoding, 2018; pp 3–7.
- (27) Sui, H.; Yao, J. Molecular simulation of CO<sub>2</sub>/CH<sub>4</sub> competitive adsorption in kerogen. *J. China Univ. Pet.* **2016**, *40*, 147–154.
- (28) Sui, H.; Yao, J. Synthesis of a New Kind Carbon Quantum Dots and Application in Copper Ion Detection. *Sci. Technol. Eng.* **2016**, *16*, 128–131.
- (29) Zhu, H.; Chang, M.; Wang, H. Study on primal CO gas generation and emission of coal seam. *Int. J. Min. Sci. Technol.* **2017**, *27*, 973–979.
- (30) Zhang, J.; Guo, L.; Zhou, X.; Wang, Y. Effect of inertinite and vitrinite of coalsamples on carbon monoxide absorption by coal seams. *J. China Coal Soc.* **2007**, *12*, 1297–1300.
- (31) Deng, J.; Cheng, F.; Song, Y.; Luo, Z.; Zhang, Y. Experimental and simulation studies on the influence of carbon monoxide on explosion characteristics of methane. *J. Loss Prev. Process Ind.* **2015**, *36*, 45–53.
- (32) Deng, J.; Luo, Z.; Wu, X.; Hu, Y. Explosive limits of mixed gases containing CH<sub>4</sub>, CO and C<sub>2</sub>H<sub>4</sub> in the goaf area. *Min. Sci. Technol.* **2010**, *20*, 557–562.
- (33) Zhou, J. *Quantum Chemistry Study on Adsorption Characteristics of CO, CO<sub>2</sub> and CH<sub>4</sub> Gas on Coal Surface*; Liaoning Technical University: Fuxin, 2012; pp 22–46.
- (34) Xu, J.; Li, X.; Wang, B.; He, J.; Lu, J. Study on primary & content and occurrence law of Coal seam in Dashuitou Coal Mine. *Min. Saf. Environ. Prot.* **2004**, *18*–20.
- (35) Wang, H. *The Study of Coal Primal CO Generation Mechanism and Adsorption, Emission Characteristics*; China University of Mining & Technology: Beijing, 2015; pp 13–22.
- (36) Zhu, H.; Chang, M.; Wang, H.; Cai, Y. Study on Existence of Coal Seam Primal CO Gas. *Coal Technol.* **2017**, *36*, 139–140.
- (37) Liang, Y.; Wang, L.; Luo, H. Law of low temperature oxidation affected to carbon monoxide generation volume during coal crushing process. *Coal Sci. Technol.* **2016**, *44*, 8–12.
- (38) Xu, Q.; Yang, S.; Tang, Z.; Cai, J.; Zhong, Y.; Zhou, B. Free Radical and Functional Group Reaction and Index Gas CO Emission during Coal Spontaneous Combustion. *Combust. Sci. Technol.* **2018**, *190*, 834–848.
- (39) Yuan, L.; Smith, A. C. Experimental study on CO and CO<sub>2</sub> emissions from spontaneous heating of coals at varying temperatures and O<sub>2</sub> concentrations. *J. Loss Prev. Process Ind.* **2013**, *26*, 1321–1327.
- (40) Zhang, J.; Jiren, W.; Chunhua, Z.; Zongxiang, L.; Jinchao, Z.; Bing, L. Molecular simulation of gases competitive adsorption in lignite and analysis of original CO desorption. *Sci. Rep.* **2021**, *11*, No. 11706.
- (41) Dong, X.; Guo, L.; Dong, X.; Wang, F. The carbon monoxide, carbon dioxide and oxygen competitive adsorption properties of Qianjiaying bituminous coals. *Coal Sci. Technol.* **2022**, No. 0125.

- (42) Zhu, H.; He, X.; Huo, Y.; Xie, Y.; Wang, W.; Fang, S. Construction and optimization of lignite molecular structure model. *J. Min. Sci. Technol.* **2021**, *6*, 429–437.
- (43) Zhang, D.; Li, Y.; Chang, L.; Zi, C.; Zhang, Y.; Tian, G.; Zhao, W. Structural characteristics of Mile lignite and its molecular model construction. *J. Fuel Chem. Technol.* **2021**, *49*, 727–734.
- (44) Wei, S.; Yan, G.; Zhang, Z.; Liu, S.; Zhang, Y. Molecular structure analysis of Jincheng anthracite coal. *J. China Coal Soc.* **2018**, *43*, 555–562.
- (45) Ge, T.; Li, Y.; Meng, W.; Li, F.; Zhang, M. Structural Characterization and Molecular Model Construction of Gas-Fat Coal With High Sulfur in Shanxi. *Spectrosc. Spectral Anal.* **2020**, *40*, 3373–3378.
- (46) Ma, R.; Zhang, S.; Hou, D.; Liu, W.; Yuan, L.; Liu, Q. Model construction and optimization of molecule structure of high-rank coal in Feng County, Shanxi Province. *J. China Coal Soc.* **2019**, *44*, 1827–1835.
- (47) Dai, J. *Quantum Chemical Calculation of the changes of Lignite Surface Active Structure at Low Temperature and Prediction of Min-Period of Spontaneous Combustion*; China University of Mining and Technology: Xuzhou, 2015; pp 22–33.
- (48) Hou, S. *The Study of Low Temperature Oxidation Process on Active Groups of Coal Molecule*; Xi'an University of Science and Technology: Xi'an, 2007; pp 59–68.
- (49) Zheng, Q.; Huang, B.; Liu, S.; Song, X.; Shi, S. Influence of Aliphatic Species on Coal Molecular Structure During Low-temperature Oxidation of Anthracite Coal. *Environ. Processes* **2020**, *7*, 159–171.
- (50) Cui, C.; Jiang, S.; Wang, K.; Zheng, S.; Li, M.; Zhang, W.; Tang, H. Effects of ionic liquid concentration on coal low-temperature oxidation. *Energy Sci. Eng.* **2019**, *7*, 2165–2179.
- (51) Yang, Y. *Mechanism and Performance of Inhibitor Based on Oxidation Characteristic of the Spontaneous Combustion of Coal*; Xi'an University of Science and Technology: Xi'an, 2015; pp 54–73.
- (52) Huang, L.; Ning, Z.; Wang, Q.; Zhang, W.; Cheng, Z.; Wu, X.; Qin, H. Effect of organic type and moisture on CO<sub>2</sub>/CH<sub>4</sub> competitive adsorption in kerogen with implications for CO<sub>2</sub> sequestration and enhanced CH<sub>4</sub> recovery. *Appl. Energy* **2018**, *210*, 28–43.
- (53) Lyu, X.; You, X.; He, M.; Zhang, W.; Wei, H.; Li, L.; He, Q. J. F. Adsorption and molecular dynamics simulations of nonionic surfactant on the low rank coal surface. *Fuel* **2018**, *211*, 529–534.
- (54) Zhou, X.; Zeng, F.; Xiang, J.; Deng, X.; Xiang, X. Macromolecular model construction and molecular simulation of organic matter in Majiliang vitrain. *CIESC J.* **2020**, *71*, 1802–1811.
- (55) Takanohashi, T.; Nakamura, K.; Terao, Y.; et al. Computer Simulation of Solvent Swelling of Coal Molecules: Effect of Different Solvents. *Energy Fuels* **2000**, *14*, 393–399.
- (56) Thompson, P. A.; Robbins, M. O. Shear flow near solids: Epitaxial order and flow boundary conditions. *Phys. Rev. A* **1990**, *41*, 6830–6837.
- (57) Meng, J.; Zhong, R.; Li, S.; Yin, F.; Nie, B. Molecular Model Construction and Study on Gas Adsorption of Zhaozhuang Coal. *Energy Fuels* **2018**, *32*, 9727–9737.
- (58) Zhang, Y.; Zhuo, J.; Wu, Y.; Yao, Q. Molecular Simulation of the Adsorption Behaviors of CO<sub>2</sub>/CH<sub>4</sub> in Curvature, Planar, and Mixture Models. *Energy Fuels* **2020**, *34*, 4153–4161.
- (59) Jiang, W.; Zhang, Q.; Cui, Y. *Mechanism Study on the Influence of CO<sub>2</sub> on CH<sub>4</sub> Adsorption on Different Rank Coals*; China Coalbed Methane, 2010; Vol. 7, pp 19–22.
- (60) Lou, H.; Jia, T. Competitive adsorption difference during coal spontaneous combustion process in noble gas atmosphere. *China Saf. Sci. J.* **2020**, *30*, 60–67.
- (61) Hu, H.; Li, X.; Fang, Z.; Wei, N.; Li, Q. Small-molecule gas sorption and diffusion in coal: Molecular simulation. *Energy* **2010**, *35*, 2939–2944.
- (62) Zhang, Y.; Shi, X.; Li, Y.; Liu, Y. Characteristics of carbon monoxide production and oxidation kinetics during the decaying process of coal spontaneous combustion. *Can. J. Chem. Eng.* **2018**, *96*, 1752–1761.
- (63) Huang, L.; Ning, Z.; Wang, Q.; Qi, R.; Zeng, Y.; Qin, H.; Ye, H.; Zhang, W. Molecular simulation of adsorption behaviors of methane, carbon dioxide and their mixtures on kerogen: Effect of kerogen maturity and moisture content. *Fuel* **2018**, *211*, 159–172.
- (64) Deng, J.; Wu, K.; Zhai, X.; Zhang, Y.; Li, P. *Simulation on Effects of CO on Coal—Oxygen Adsorption Process*; Safety in Coal Mines, 2011; Vol. 42, pp 16–19.